Anal Bioanal Chem
DOI 10.1007/s00216-015-8636-z

RESEARCH PAPER

pH sensitivity of FRET reporters based on cyan and yellow fluorescent proteins

Dahdjim-Benoît Betolngar[1] · Marie Erard[1] · Hélène Pasquier[1] · Yasmina Bousmah[1] · Awa Diop-Sy[1] · Elvire Guiot[2] · Pierre Vincent[2] · Fabienne Mérola[1]

Received: 3 February 2015 / Revised: 10 March 2015 / Accepted: 12 March 2015

Abstract It is generally acknowledged that the popular cyan and yellow fluorescent proteins carried by genetically encoded reporters suffer from strong pH sensitivities close to the physiological pH range. We studied the consequences of these pH responses on the intracellular signals of model Förster resonant energy transfer (FRET) tandems and FRET-based reporters of cAMP-dependent protein kinase activity (AKAR) expressed in the cytosol of living BHK cells, while changing the intracellular pH by means of the nigericin ionophore. Although the simultaneous pH sensitivities of the donor and the acceptor may mask each other in some cases, the magnitude of the perturbations can be very significant, as compared to the functional response of the AKAR biosensor. Replacing the CFP donor by the spectrally identical, but pH-insensitive Aquamarine variant ($pK_{1/2}$=3.3) drastically modifies the biosensor pH response and gives access to the acid transition of the yellow acceptor. We developed a simple model of pH-dependent FRET and used it to describe the expected pH-induced changes in fluorescence lifetime and ratiometric signals. This model qualitatively accounts for most of the observations, but reveals a complex behavior of the cytosolic AKAR biosensor at acid pHs, associated to additional FRET contributions. This study underlines the major and complex impact of pH changes on the signal of FRET reporters in the living cell.

Keywords FRET · Biosensor · FLIM · AKAR · Aquamarine · Citrine

Electronic supplementary material The online version of this article (doi:10.1007/s00216-015-8636-z) contains supplementary material, which is available to authorized users.

✉ Fabienne Mérola
fabienne.merola@u-psud.fr

[1] CNRS, Laboratoire de Chimie Physique, UMR 8000 and Université Paris-Sud, Avenue Jean Perrin 15, 91405 Orsay, France

[2] CNRS, Biological Adaptation and Ageing, UMR 8256 and Université Pierre et Marie Curie, Place Jussieu 4, 75252 Paris, France

Introduction

Green fluorescent protein variants (GFPs), combined with genetic fusion techniques and the Förster resonant energy transfer (FRET) mechanism, provide a generic and flexible framework for the engineering of dedicated live cell reporters of ions, metabolites, enzymatic activities, molecular interactions, or transmembrane transports, with ever expanding applications in cell biology, biotechnology, and medical research [1, 2]. In the vast majority of cases, these reporters carry a cyan fluorescent protein (such as ECFP or Cerulean) and a yellow fluorescent protein (such as EYFP or Citrine), respectively, playing the roles of donor and acceptor of the energy transfer. The fluorescent proteins are usually grafted either on two separate proteins of interest, whose molecular proximity needs to be assessed, or on the two termini of a protein sensor module, that is engineered to undergo a major conformational change (or hydrolysis) in response to a biochemical event. Owing to specific peptidic sequences, these genetically encoded FRET reporters bear the unique ability to be targeted to extremely precise subcellular locations.

To the exception of a few blue and red fluorescent proteins, the fluorescence of most GFPs used for biological imaging display strong sensitivities to pH and other ions [3]. This sensitivity has been exploited for the development of targetable pH or chloride sensors [4–7], which have contributed a wealth of detailed information on subcellular pH regulation in a variety of organelles [8]. Yet, this pH sensitivity potentially

Published online: 27 March 2015

remains a major flaw when biochemical activities other than pH need to be assayed. Indeed, although the intracellular pH is a highly regulated parameter, the local pH value can substantially vary along normal or pathological metabolism, not only during secretory organelle maturation [8], endocytosis, and phagocytosis [9], or as a result of respiratory activity in mitochondria [10], but also in the vicinity of active transmembrane currents or as a secondary effect of calcium release from calcium stores [11, 12]. Significant intracellular pH gradients are building up during cell migration [13], and changes in the intracellular pH are associated to apoptosis [14] and ischemia [15]. These pH changes can lead to significant perturbations of the fluorescence signals of genetically encoded FRET reporters, and there is a need to evaluate, and correct as much as possible, for these pH effects.

The differences in pH sensitivity of CFPs and YFPs carried by a single-chain tandem FRET construct were used to develop a series of ratiometric pH sensor called pHlameleons [7]. On the other hand, Salonikidis et al. compared the ECFP/EYFP and Cerulean/Citrine FRET pairs carried by a biosensor of cAMP (EPAC) in cell lysates, over a wide range of pHs and ion concentrations [11]. By use of linear unmixing of fluorescence emission spectra, they achieved a separation of the respective donor and acceptor pH responses in EPAC. Several new cyan fluorescent proteins, such as mCerulean3 [16], mTurquoise2 [17], and Aquamarine [18], were recently engineered, which display, besides an enhanced fluorescence quantum yield approaching unity, and near-single exponential fluorescence emission decays, a distinctive pH stability of their fluorescence, with a $pK_{1/2}$ below 3.5. These new cyan forms are spectrally identical to, and can thus readily replace, the usual ECFP or Cerulean donors in FRET constructs [19]. In particular, the Aquamarine variant differs from ECFP by the mutation of only two residues buried in the chromophore pocket. Exchanging ECFP for Aquamarine thus allows a direct transformation of the donor within a FRET construct, from a pH sensitive to a non-pH sensitive one, with minimum otherwise structural perturbations.

In the present study, we take this opportunity to decipher the pH responses of cyan-yellow FRET systems in the living cell. Combining live cell fluorescence lifetime imaging microscopy (FLIM) and established methods to manipulate the intracellular pH, we quantify the pH-dependent FRET efficiencies in cyan-yellow FRET tandems and in a biosensor of cAMP-dependent kinase activity (AKAR). By comparing experimental data with the predictions of a simple model of pH-dependent energy transfer, we analyze in detail the donor and acceptor contributions to fluorescence lifetime changes. We also extend our model to predict the effects of similar pH changes on the ratiometric signal of the biosensor. This work represents a first attempt to decipher the pH effects along live cell FRET imaging experiments.

Materials and methods

Molecular biology, biochemistry, and spectroscopy studies

ECFP refers to *Av*GFP F64L/S65T/Y66W/N146I/M153T/V163A/H231L (Clontech), and EYFP to *Av*GFP-S65G-V68L-S72A-T203Y. Aquamarine (ECFP-T65S-H148G), Citrine (EYFP-Q69M), the mutation T65S in Cerulean, and the non-chromophoric Y66A versions of yellow fluorescent proteins were obtained by single or multiple rounds of site-directed mutagenesis of the corresponding plasmids using the QuickChange mutagenesis kit from Stratagene.

For cytosolic expressions, the pECFP-N1 plasmid (Clontech) was used. The pECFP-EYFP tandem fusion contained ECFP and EYFP separated by a linker of 27 amino acids (sequence SGLRSASVDTMGRDLYDDDDKDPPAEF) [20]. The AKAR2.2 and the AKAR4 biosensors cloned in pCDNA3 were generous gifts from Jin Zhang (The Johns Hopkins University School of Medicine, Baltimore, USA) and were used as received. The CFP of AKAR2.2 carries the mutations K26R, N164H, and A206K and is deleted from its last 11 C-terminal amino acids. The Citrine of AKAR2.2 carries the mutations A206K and H231L. All sequences were checked by DNA sequencing.

For bacterial expression, EYFP and Citrine were cloned in pProExHTa to produce a His-tagged protein (Invitrogen) and were purified as previously described [18]. The absorption and fluorescence properties of purified EYFP and Citrine were studied at 25 °C with a multiwell plate reader. Buffer solutions contained 30 mM CAPS, 30 mM MES, and 30 mM Bis–tris propane for pH levels ranging from 11 to 5.5, and 50 mM citric acid for pH levels ranging from 5.5 to 2.5. Buffers were adjusted to the appropriate pH by addition of H_2SO_4 or NaOH. Aliquots from a concentrated stock protein solution were diluted into the different buffers at least 12 h before measurements.

Cell cultures and transfections

Baby hamster kidney cells (BHK-21) were cultivated in MEM Glutamax (Invitrogen) supplemented with 5 % FCS in 25 cm^2 flasks. For microscopy, cells were grown to 80 % confluence on 25 mm (FLIM) or 10 mm (ratiometry) Ø glass coverslip and transfected with the expression plasmids using Lipofectamine 2000 (Life technology) following the manufacturer's protocol. Cells were studied 24 to 48 h after transfection.

Intracellular pH changes with nigericin

The cytosolic pH of BHK cells expressing the appropriate plasmid was modified by a method based on the K^+/H^+ ionophore nigericin in the presence of external potassium ions [21]. The nigericin K^+/H^+ antiporter rapidly and reversibly

equilibrates the external and internal pH of the cell, including all subcellular compartments, such as secretion granules [22]. This method is widely used for the intracellular calibration of synthetic [23] and genetically encoded [24] fluorescent pH indicators. Cells were bathed in an observation medium MES (15 mM) HEPES (15 mM) containing 140 mM KCl and 13 μM nigericin, adjusted at the desired pH.

In FLIM imaging, the fluorescence lifetime of individual cells was first determined at pH 7.4, the observation medium was then removed by pipetting and replaced by a buffer equilibrated at a different pH, and the fluorescence lifetime was measured again on the same cells whenever possible. In ratiometry imaging, the cells were continuously perfused with the observation medium heated at 32 °C. Images were first collected for 5–10 min while flowing a buffer at pH 7.4, then the perfusion was switched to another reservoir at acid pH for about 10–15 min, and the cells were finally rinsed back with the original buffer. In the case of cells expressing the AKAR biosensor, acid pH levels sometimes elicited the formation of punctate fluorescent granules, which disappeared when the pH was changed back to neutral, an observation also reported by Salonikidis et al. in the case of the EPAC biosensor [11]. As these fluorescent granules correspond to regions of high fluorophore density, they might be associated to elevated levels of non-specific, bystander FRET [20]. These regions were avoided as much as possible during data processing.

FLIM experiments and data analysis

FLIM was performed by the technique of time-correlated single photon counting (TCSPC), on a homemade setup as previously described [24]. The system is based on an inverted TE2000 microscope equipped with a ×60, 1.2 NA water immersion objective (Nikon, Japan). The excitation source was a PicoQuant LDH 440 pulsed diode laser of 80 ps FWHM, operated at 20 MHz repetition rate (PicoQuant, Berlin, Germany), giving a final power <1 μW at 442 nm on the sample. The excitation beam was scanned onto the sample by means of a Nikon C1 laser-scanning head. The sample fluorescence was diverted by a 45° dichroic mirror (SWP-500, Lambda Research Optics), completed by a double set of rejection filters (458 nm Razor Edge Long pass, Semrock, Rochester, NY, USA) and a CFP filter (480AF30, Omega Optical, Brattleboro, VT, USA). The TCSPC detection consisted of a MCP-PMT detector (Hamamatsu, Japan) and fast timing electronics (PicoHarp 300, PicoQuant) driven by the SymPhoTime 5 software. The FLIM setup is completed by a camera imaging port equipped with a cooled CCD camera (ORCA-AG, Hamamatsu). This port is used to collect wide-field fluorescence images of the samples under HBO lamp illumination controlled by a fast shutter (Uniblitz, Vincent and Associates, Rochester, NY, USA). Two wide-field fluorescence images of the same sample area studied by FLIM are collected, respectively, through a CFP filter cube (Omega XF114-2) and a YFP filter cube (Omega XF105-2). These images are used to control the cyan and yellow fluorophore levels corresponding to the FLIM measurements. All measurements were performed at 20±1 °C, by means of a circulating water temperature bath. Photobleaching and contaminations by autofluorescence and bystander FRET [20] were all kept to negligible levels by dedicated controls.

The SymPhoTime software calculates the intensity image of the scanned field of view and the TCSPC fluorescence decay of ROIs containing 2–6 10^6 cts is exported for further decay analyses with a homemade routine coded in IGOR Pro (Wavemetrics, Lake Oswego, OR, USA). Tail-fitting, multiexponential fits of the fluorescence decays were performed, and the average lifetime corresponding to the best residuals and chi-square was computed as $\tau=\sum c_i\tau_i$ were c_i and τ_i are respectively the individual lifetimes and normalized pre-exponential amplitudes ($\sum c_i=1$). For each fluorescent construct and each pH condition, averages and standard deviations of measurements from a minimum of 5 to 15 different cells are reported.

Ratiometry experiments and data analysis

Ratiometry imaging was performed on a previously described homemade setup [25] based on an upright microscope (Olympus BX51WI) equipped with a ×40 0.8 NA or a ×60 0.9 NA water immersion objectives, a piezoelectric device (P-721 PIFOC, Physik Instrumente GmbH) to remotely control image focus. The observation chamber is perfused continuously with the observation medium. The installation has five different reservoirs for changing the observation medium without touching the sample. Epifluorescence is excited using a halogen light source, controlled by a fast shutter (Uniblitz, Vincent and Associates, Rochester, NY), and a D436/20 filter for excitation. A 455DCXT dichroic mirror separates the emission from the excitation. The emitted light is filtered by alternating the emission filters, HQ480/40 for CFP and D535/40 for YFP, with a filter wheel (Sutter Instruments, Novato, CA, USA), and images are recorded with a low noise CCD camera (ORCA-AG, Hamamatsu). Filters were obtained from Chroma Technology (Bellows Falls, VT, USA) or Semrock. All setup elements are controlled through the iVision software (BioVision). The acquired images are immediately processed in IgorPro (WaveMetrics) via a homemade procedure, to yield an experimental FRET ratio F535/F480 corrected for background, exposure times, and field inhomogeneities [25].

Results and discussion

pH responses of purified cyan and yellow fluorescent proteins

The behavior of a FRET system depends first on the respective photophysical responses of its donor and acceptor fluorophores. We summarize below the different pH-induced perturbations observed in the spectroscopic properties of purified cyan and yellow fluorescent proteins. When necessary, experiments aimed at complementing the available literature have been performed and are reported in detail in the Electronic Supplementary Material (ESM).

At near physiological pH, green and yellow fluorescent proteins undergo a reversible protonation of their anionic chromophore, leading to the formation of a neutral, usually non-fluorescent form, with a blue-shifted absorption spectrum [4, 5]. The protonation pK of YFPs is strongly influenced by halide or nitrate ions [26], while Citrine and Venus, two improved yellow versions, are reportedly insensitive to these anions [27, 28]. The halide sensitivity of YFPs mostly stems from a 1:1 binding of small anions near the chromophore, which alters its protonation equilibrium [6]. We have reassessed the absorption and fluorescence properties of purified EYFP and Citrine at different pH levels and chloride concentrations (see ESM). In the absence of chloride anions, the half-transition point for chromophore protonation is identical for both proteins: $pK_{1/2}$=5.6±0.1. The $pK_{1/2}$ of EYFP rapidly increases in the presence of low concentrations of chloride anion, reaching $pK_{1/2}$=6.7 at 100 mM KCl, with an asymptotic limit above pH 7 when the chloride concentration is further increased (Fig. 1). We find that the protonation $pK_{1/2}$ of Citrine also increases, yet more slowly, with chloride concentration and tends towards an asymptotic value close to pH 6 (Fig. 1).

The fluorescence intensity of EYFP and Citrine decreases with decreasing pH, closely following the loss in their anion absorbance (see ESM Fig. S1). Meanwhile, the anion absorption and emission spectral band shapes remain unchanged, indicating the absence of major structural perturbations during protonation. However, when going to lower pHs, the fluorescence lifetime of EYFP and Citrine decreases, with approximate $pK_{1/2}$ of 4.4±0.1 for EYFP and 4.7±0.1 for Citrine (see ESM Fig. S2), a dynamic quenching that might reflect the onset of some acid denaturation. Indeed, the absorption spectra of EYFP and Citrine measured at pH 3.5 and below display a quite different absorption peak, with a maximum at 380 nm, indicating a non-native chromophore environment.

The pH sensitivity of cyan fluorescent proteins has long been overlooked, in view of the strong pH responses of their yellow partners, and also because their tryptophan-based chromophore is not expected to change its protonation state at physiological pH levels. Yet, the fluorescence intensity and lifetime of purified ECFP and Cerulean decrease markedly at acid pH [29], a phenomenon that is readily detectable also in the living cell [18, 24]. The absorption and fluorescence properties of ECFP and Cerulean as a function of pH have been analyzed in detail in previous work [29]. While the absorption of ECFP undergoes only limited perturbations from pH 11 down to pH 5, its fluorescence intensity decreases with $pK_{1/2}$=5.6 (n_{Hill}=0.7±0.1), which is paralleled by a similar decrease of its average fluorescence lifetime. During this transition, the ECFP emission spectrum slightly changes its shape, but remains essentially centered on the same wavelength range [29]. The absorption and fluorescence properties of ECFP, as well as their pH dependence, are insensitive to the presence of chloride. Introducing the two mutations T65S and H148G in ECFP leads to the Aquamarine variant, whose fluorescence properties are completely insensitive to pH down to pH 4, where a highly cooperative transition starts to take place ($pK_{1/2}$=3.3) [18].

Therefore, acid-induced perturbations arise from quite different mechanisms in cyan and yellow fluorescent proteins. In the case of ECFP and Cerulean, the major event taking place is an increase of the dynamic quenching of the fluorescence. We speculated that this quenching stems from an increased rate of excited state chromophore torsions, due to a softening of the local protein structure under acidic conditions [29], while a better blockage of these excited state torsions would be achieved in Aquamarine. In the case of yellow fluorescent proteins, the major event at acidic pH is a loss of ground state anion absorbance, due to chromophore protonation, which is accompanied by little changes of its characteristic absorption

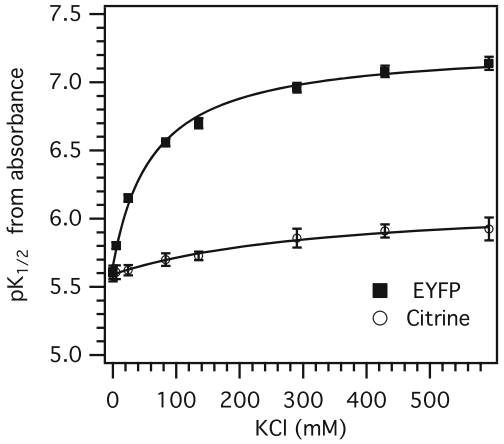

Fig. 1 Chromophore protonation pK of purified yellow fluorescent proteins as a function of chloride concentration. The chromophore $pK_{1/2}$ of EYFP (*black squares*) and Citrine (*empty circles*) were obtained from studies of their absorption spectra as a function of pH performed at varying KCl concentrations (see ESM). Continuous lines represent best fits of the data to a saturation hyperbole: $pK_{1/2}[KCl] = \frac{pK_{max}[KCl] + pK_{min} \times K_{app}}{[KCl] + K_{app}}$ giving the respective parameters: pK_{min}=5.65±0.04, pK_{max}=7.27±0.05, K_{app}=63±10 mM for EYFP, and pK_{min}=5.59±0.01, pK_{max}=6.14±0.06, K_{app}=350±100 mM for Citrine

and emission properties. At pH levels below 6, we find also evidence for the onset of some dynamic quenching of the YFP fluorescence. By contrast with chromophore protonation, but similarly to the acid quenching of CFPs, this process appears insensitive to chloride, as shown by comparable experiments on EYFP in the presence of 150 mM NaCl [30].

These different pH-dependent perturbations will first directly modify the fluorescence signals of genetic constructs carrying cyan and yellow fluorescent proteins. In addition, according to Förster's theory, a decrease in donor quantum yield and acceptor absorbance will markedly decrease the FRET efficiency, and thus the chemical sensing ability of the FRET reporter. Because of the large variations in intracellular chloride concentrations [31], the effective $pK_{1/2}$ of YFP chromophore protonation is also poorly defined in the living cell. For all these reasons, the precise consequences of pH changes along FRET imaging experiments remain difficult to anticipate solely from the above solution studies. Therefore, we carried out a systematic FLIM study of intracellular FRET constructs as a function of pH.

pH responses of cytosolic FRET tandems

Fluorescence lifetime imaging (FLIM) is a powerful technique for accurate quantitative investigations of FRET, as the energy transfer efficiency E_{FRET} can be readily determined from the average fluorescence lifetimes of the donor in the presence (τ_{DA}) and absence (τ_D) of the acceptor, through the well-known relationship $E_{FRET}=1-(\tau_{DA}/\tau_D)$ [20]. We first studied by FLIM different cytosolic tandem constructs composed of a pair of cyan and yellow fluorescent proteins, connected by a short linker of 27 amino acids. Such tandems are widely used as positive controls in live cell FRET imaging studies. The nature of the donor and the acceptor was varied, and the donor fluorescence lifetime was measured by TCSPC-FLIM, while imposing a range of intracellular pH levels comprised between pH 8.5 and pH 5, using incubation buffers containing the nigericin ionophore (see "Materials and methods"). The results of these experiments are shown in Fig. 2.

The ECFP-EYFP tandem expressed in the neutral cytosol of living cells has been extensively characterized in a previous study [20]. The ECFP fluorescence lifetime in this tandem is markedly decreased as compared to free cytosolic ECFP (Fig. 2), indicating a significant FRET interaction between the cyan and yellow moieties. Introducing the Y66A mutation into the EYFP acceptor leads to a structurally equivalent construct, noted ECFP-EYFP(Y66A), which is devoid of any acceptor chromophore and provides a good reference for FRET quantifications [20]. The fluorescence lifetime of this "donor-only" control is close to that measured for cytosolic ECFP (Fig. 2). A FRET efficiency of 32 % is determined at pH 7.4, in good agreement with previous determinations [20].

Quite deceptively, the donor fluorescence lifetime of the ECFP-EYFP tandem appears only weakly sensitive to the intracellular pH (Fig. 2). By contrast, the fluorescence lifetime of the donor-only construct ECFP-EYFP(Y66A) undergoes a marked decrease at acid pHs (Fig. 2). The pH sensitivity of the cyan donor inside the tandem is fairly similar to that of free cytosolic ECFP (Fig. 2), with a transition point $pK_{1/2}=6.10\pm0.07$, a value significantly higher than for the purified ECFP protein. Comparing the fluorescence lifetimes of the full ECFP-EYFP tandem and the donor-only control shows that the FRET efficiency actually drops to zero near pH 5.5 (Fig. 2).

The fluorescence lifetime of cytosolic Aquamarine remains unchanged over a large range of pH levels, with a mean value of 3.91±0.06 ns between pH 8.5 and pH 5 (Fig. 2), in agreement with our previous report [18]. The Aquamarine fluorescence lifetime is also mostly insensitive to genetic fusion to other proteins, as well as to subcellular targeting [18]. We replaced the ECFP donor in our tandem by the pH-insensitive Aquamarine and studied similarly the cytosolic construct Aqua-EYFP as a function of intracellular pH. From the fluorescence lifetimes measured on Aqua-EYFP and on cytosolic Aquamarine (Fig. 2), we estimate a FRET efficiency of 38 % for Aqua-EYFP at neutral pH. When going from pH 7.4 to pH 5, the Aquamarine lifetime in Aqua-EYFP undergoes a pronounced 40 % increase (Fig. 2). We hypothesize that this increase primarily reflects the pH sensitivity of the EYFP acceptor. As expected, replacement of the EYFP acceptor by a Citrine displaces the apparent transition to more acidic

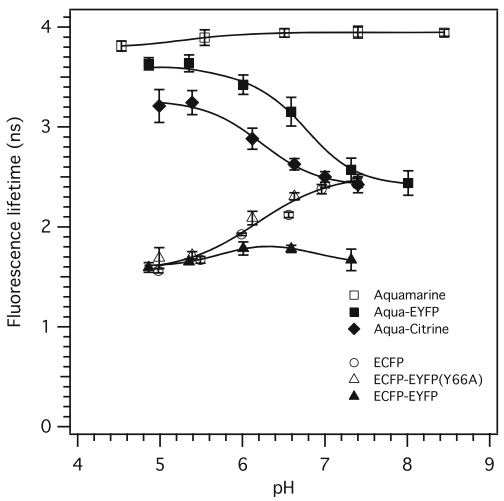

Fig. 2 Fluorescence lifetime of the cyan donor of FRET tandems as a function of the intracellular pH. The different tandems were transiently expressed in the cytosol of living BHK cells. The average donor lifetimes were determined by TCSPC-FLIM (T=20±1 °C), and the cytosolic pH was modified by changing the extracellular medium in the presence of the nigericin ionophore (see "Materials and methods"). Each data point is the average of 5 to 22 measurements on different cells, and the standard deviations on these repeated measurements are shown. The continuous lines are for eye guidance only

pH levels, from $pK_{1/2}$=6.7±0.1 in the case of Aqua-EYFP to $pK_{1/2}$=6.2±0.1 in the case of Aqua-Citrine (Fig. 2). Again, these transitions take place at substantially higher pH levels than for the purified proteins. The obtained values are quite comparable to those determined by Salonikidis et al. for YFP ($pK_{1/2}$=7.2) and Citrine ($pK_{1/2}$=5.9) attached to the EPAC biosensor in cell lysates in the presence of 140 mM chloride [11].

Taken together, these results illustrate how the respective pH sensitivities of cyan and yellow fluorescent proteins make distinct and opposite contributions to the donor FLIM signal in a FRET system. While the ECFP donor fluorescence lifetime tends to decrease with decreasing pH, this effect is opposed by the loss in acceptor absorbance and concomitant release of the FRET quenching. If the two events take place over similar pH ranges, they may compensate each other, resulting in a nearly stable donor fluorescence lifetime, as in our ECFP-EYFP tandem. A relatively stable fluorescence intensity of the ECFP donor was also reported by Salonikidis et al. for the EPAC biosensor at acid pH levels, while the yellow acceptor signal was at the same time rapidly decreasing [11]. In these conditions, any FRET-based biochemical sensing will be considerably, if not totally compromised, as the FRET interaction itself is vanishing. Replacing the ECFP donor by a pH-insensitive fluorophore like Aquamarine clearly reveals the collapse of the yellow acceptor.

pH responses of AKAR biosensors in their basal state

The cAMP-dependent kinase sensor AKAR2.2 bears a CFP as the FRET donor, and a Citrine as the acceptor, grafted around a phosphoamino acid binding domain (FHA) and a PKA-specific substrate sequence [32]. We studied the FLIM signal of the CFP donor of AKAR2.2 in its basal state, together with that of a donor-only version, AKAR2.2(Y66A), as a function of the intracellular pH. The results are shown in Fig. 3.

In the donor-only construct AKAR2.2(Y66A), the CFP fluorescence lifetime undergoes a marked and cooperative decrease when going from basic to mildly acid pH levels ($pK_{1/2}$=6.6, n_{Hill}=1.7), a behavior that clearly differs from that of cytosolic ECFP (Figs. 2 and 3). The increased pH sensitivity of CFP in AKAR2.2(Y66A) thus reflects a specific perturbation of the fluorescent protein associated to its incorporation into the biosensor. It is worth noting that the sequence of the CFP of the AKAR2.2 biosensor is not strictly identical to that of ECFP (see "Materials and methods"). In the same pH range, the CFP donor lifetime of AKAR2.2 carrying an intact Citrine acceptor also undergoes a marked decrease (Fig. 3). A comparison of AKAR2.2 and its donor-only version shows that the moderate FRET efficiency of the biosensor at neutral pH (19 % at pH 7.4) decreases but does not completely cancel out at pH 5 (Fig. 3).

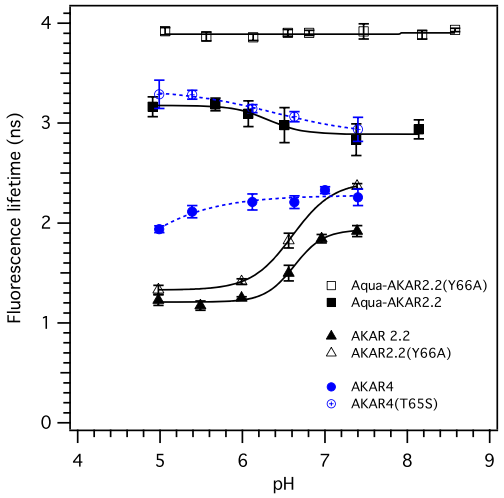

Fig. 3 Fluorescence lifetime of the cyan donor of AKAR biosensors as a function of the intracellular pH. The different biosensors were transiently expressed in the cytosol of living BHK cells. The average donor lifetimes were determined by TCSPC-FLIM (T=20±1 °C), and the cytosolic pH was modified by changing the extracellular medium in the presence of the nigericin ionophore (see "Materials and methods"). Each data point is the average of 5 to 35 measurements on different cells, and the standard deviations on these repeated measurements are shown. The continuous lines are for eye guidance only

We introduced the T65S and H148G mutations into the CFP donor of the biosensor, leading to the Aqua-AKAR2.2 construct and its donor-only version Aqua-AKAR2.2(Y66A). We already reported that the modified biosensor Aqua-AKAR2.2 can be used similarly to the original sensor, to monitor forskolin-induced PKA activation in BHK cells [18]. In the donor-only construct Aqua-AKAR2.2(Y66A), the Aquamarine fluorescence lifetime is identical to that of cytosolic Aquamarine, and is similarly insensitive to the intracellular pH, with an average value of 3.90±0.03 ns between pH 8.5 and pH 5 (Fig. 3). In the same pH range, the Aquamarine lifetime of the Aqua-AKAR2.2 biosensor carrying an intact Citrine acceptor increases slightly from 2.94 to 3.16 ns (Fig. 3). Accordingly, the FRET efficiency of the biosensor slightly decreases, but remains significant at acidic pH (from 25 % at pH 7.4 to 19 % at pH 5).

AKAR4 is a more recent version of AKAR that carries a Cerulean as the cyan donor and a circularly permuted Venus as the yellow acceptor [33]. By contrast to AKAR2.2, the fluorescent lifetime of the Cerulean donor of AKAR4 only slightly decreases when going to acid pH levels (Fig. 3). The single point mutation T65S was shown to convert the pH-sensitive Cerulean into a pH-insensitive cyan fluorescent protein very similar to Aquamarine [29]. When the mutation is introduced into Cerulean, the fluorescence lifetime of AKAR4-T65S now slightly increases on the contrary at acid pH levels, quite similarly to Aqua-AKAR2.2 (Fig. 3).

pH effects on the AKAR ratiometric traces

FRET ratiometry imaging typically consists in measuring the spatio-temporal variations of the ratio R_{FRET} between acceptor and donor fluorescence emission intensities, while exciting the donor near its maximum of absorption. Ratiometry is the most popular method for monitoring the response of single-chain FRET biosensors because of its simplicity and high sensitivity. It is therefore interesting to evaluate the consequences of pH-induced perturbations on a biosensor ratiometric signal. An average ratiometric trace of AKAR2.2 during a transient change of the intracellular pH from pH 7.5 to pH 5 is shown in Fig. 4. Decreasing the cytosolic pH induces a marked decrease of the intensity in both donor and acceptor channels, accompanied by a 36±13 % (N=9) decrease of the FRET ratio. When the pH is restored to its initial value, the ratio approximately reverts back to its basal level (Fig. 4). The magnitude of this pH-induced perturbation is very significant compared to the usual response of cytosolic AKAR2.2 to PKA activation by forskolin (typically $\Delta R/R \approx +$ 10–20 %, [25]. This strong pH effect is not specific to the AKAR2.2 biosensor. In response to the same pH change, we observe similar negative and reversible variations of the FRET ratio in the case of a simple ECFP-Citrine tandem ($\Delta R/R = -40\pm5$ %, N=18) and in the case of AKAR4 ($\Delta R/R = -32\pm$ 8 %, N=12). In the later case, the change in FRET ratio corresponds to nearly half the maximum response reported for AKAR4 to PKA activation ($\Delta R/R$=+68 %) [33]. Salonikidis et al. observed also very large drops in the FRET ratio of their EPAC biosensors, when going from neutral to acid pH levels [11].

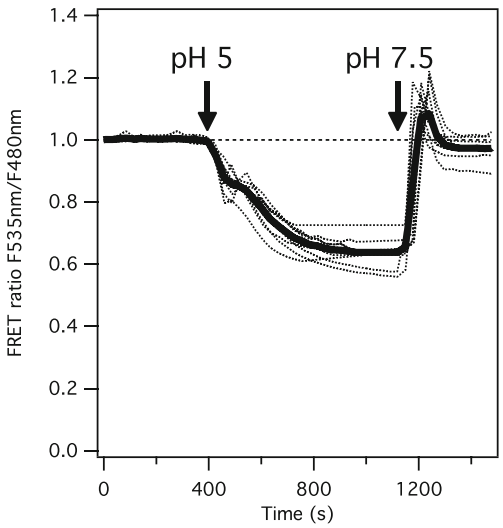

Fig. 4 Variation of the basal FRET ratio of the AKAR2.2 biosensor upon a change in the cytosolic pH of living BHK cells. *Thick line*, average trace computed from individual cell experiments (*dotted lines*, N=9). The cells were initially bathed with a circulating neutral buffer, and the cytosolic pH was modified at the indicated time points (*arrows*), by changing the circulating medium in the presence of nigericin (see "Materials and methods")

These results show that pH variations can have a major impact on the ratiometric traces of biosensors, as compared to their maximum functional responses. It is also important to note that, in the presence of such pH variations, the use of different detection techniques (FLIM or ratiometry) can actually lead to quite different and possibly opposite conclusions regarding the "activation" state of the biosensor. For example, the decreased FRET ratio of AKAR2.2 (Fig. 4) might be erroneously interpreted as a decreased kinase activation level, while the decreased fluorescence lifetime of the same biosensor (Fig. 3) would be interpreted on the contrary as an increased activation state.

Modeling the pH responses of FLIM signals

The fluorescence lifetimes of our tandems and biosensors respond as qualitatively expected from the pH dependence of their respective donors and acceptors. Yet, different FRET tandems and biosensors behave quite differently, suggesting specific contributions from the construct itself. To improve our understanding of these effects, we developed a simplified model of pH-dependent donor lifetimes in a FRET system which is described in the ESM.

The model relies on basic Förster theory and assumes simple acid-base transitions of (i) the fluorescence lifetime of the CFP donor between the values τ_D^{basic} and τ_D^{acid} around the half-transition point pK_D and (ii) the absorption of the YFP acceptor around the half-transition point pK_A. Each donor-acceptor system is also characterized by a specific FRET efficiency at basic pH levels, obtained from the measured values of the donor lifetime at these pH levels in the absence (τ_D^{basic}) and presence (τ_{DA}^{basic}) of the acceptor. This FRET efficiency is characteristic of the spatial organization of the construct that is assumed unchanged during the acid transition. These principles lead to the following expressions (see ESM):

$$\tau_D(pH) = \frac{\tau_D^{basic} + 10^{n_{Hill}^{*}(pK_D - pH)}\tau_D^{acid}}{1 + 10^{n_{Hill}^{*}(pK_D - pH)}} \quad (1a)$$

$$k_{FRET}(pH) = \frac{\left(\frac{1}{\tau_{DA}^{basic}} - \frac{1}{\tau_D^{basic}}\right)}{1 + 10^{(pK_A - pH)}} \quad (1b)$$

$$\tau_{DA}(pH) = \frac{1}{\frac{1}{\tau_D(pH)} + k_{FRET}(pH)} \quad (1c)$$

τ_D^{basic}, τ_D^{acid}, n_{Hill}, and pK_D are obtained experimentally from the donor-only control, and τ_{DA}^{basic} from the FRET construct at pH 7.4 (see ESM Table S2). The theoretical donor lifetimes $\tau_D(pH)$ and $\tau_{DA}(pH)$ are then computed as a function of pH according to Eqs. 1a–c.

The results of these numerical simulations for the ECFP-EYFP tandem are shown in the lower part of Fig. 5. For the ECFP donor, we used pK_D=6.2 as determined for cytosolic ECFP (triangles). For the EYFP acceptor, we tried a range of pK_As ranging from 5.6 to 7.0 (series of continuous and dashed lines). If $pK_A<pK_D$, the donor lifetime τ_{DA} goes through a faint minimum when going from neutral to acid pH. When $pK_A>pK_D$, a transient increase of τ_{DA} takes place, which becomes more pronounced when the donor and acceptor transitions become more separated. The simulations obtained for the tandems carrying Aquamarine instead of ECFP are displayed in the upper part of Fig. 5. For these simulations, we assumed the pK_D=3.3 of purified Aquamarine. Due to this very acidic value, the pK_A of the acceptor is always higher than the donor pK_D, and a marked transient maximum is observed in all cases for τ_{DA}(pH) (Fig. 5). On the whole, we obtain model pH responses for the different tandems quite similar to the experimental observations, assuming a pK_A in the range 6.5–6.7 for EYFP and a pK_A close to 6.2 for Citrine (Fig. 5). The agreement is less satisfactory below pH 6, where several approximations of our simple model may be less valid (see ESM). No attempt was made at the moment to refine our theoretical description.

We then tried to describe similarly the pH dependence of the donor fluorescence lifetime in the AKAR constructs, which resulted in the simulations shown in Fig. 6. As pointed above, the pH sensitivity of the CFP donor in AKAR2.2(Y66A) is characterized by a cooperative transition (n_{Hill}=1.7) with pK_D≈6.6. For the FRET system AKAR2.2 (lower series of continuous and dashed lines in Fig. 6), assuming a range of different pK_As for the Citrine acceptor gives rise to a series of curves quite similar to the experimental observations, but all very close from each other, which forbids any precise evaluation of the acceptor pK_A. In the case of Aqua-AKAR2.2, the experimental observations cannot be described by any of our model curves: while our model predicts a recovery of the Aquamarine lifetime at acidic pH, it is clearly not the case for the experimental lifetime, which slightly increases around pH≈6.3 and then stays at a persistently low value down to pH 5 (Fig. 6). This behavior clearly indicates the occurrence of a different pH-dependent process governing the FRET level in Aqua-AKAR2.2.

Modeling the pH responses of ratiometric traces

We tried also to evaluate the expected evolution of FRET ratiometric traces in the presence of pH changes. In a typical ratiometric experiment with cyan/yellow fluorescent protein FRET pairs, the intensity I_D measured in the "donor" channel is usually assumed to monitor the pure signal of the FRET-quenched donor, while the intensity I_A detected in the "acceptor" channel is expressed as the sum of (i) the FRET-sensitized acceptor fluorescence (I_{sA}), (ii) the directly excited acceptor fluorescence (I_{dA}), and (iii) the donor bleed through (I_{bD}) [34–36]. From these commonly accepted principles, the

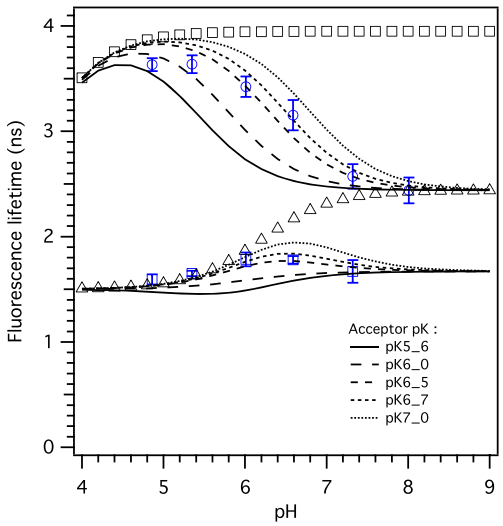

Fig. 5 Numerical simulations of the cyan donor fluorescence lifetime at different pH levels in FRET tandems. The model assumes independent pH transitions of the donor fluorescence lifetime and of the acceptor absorbance, and τ_{DA}(pH) is computed according to Eq. (1). The computed lifetimes of the cyan donor alone in the absence of acceptor are displayed as *triangles* (ECFP) and *squares* (Aquamarine), and a series of pK_A values ranging from 5.6 to 7.0 was tested for the yellow acceptor (*continuous and dashed lines*). The experimental data for ECFP-EYFP (*blue squares*) and Aquamarine-EYFP (*blues circles*) is reproduced from Fig. 2. All parameters used for the simulations are given in ESM Table S2

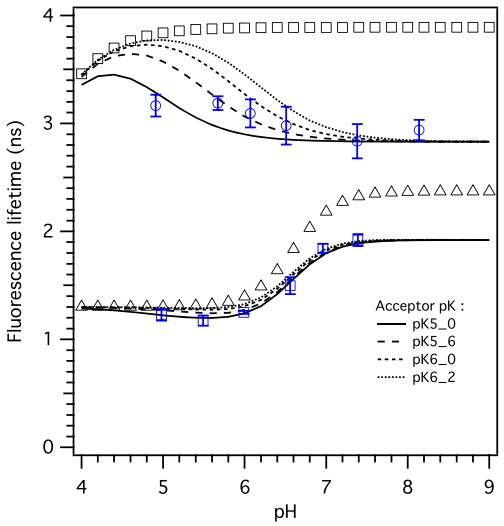

Fig. 6 Numerical simulations of the cyan donor fluorescence lifetime at different pH levels in AKAR biosensors. The model assumes independent pH transitions of the donor fluorescence lifetime and of the acceptor absorbance, and τ_{DA}(pH) is computed according to Eq. (1). The computed lifetimes of the cyan donor alone in the absence of acceptor are displayed as *triangles* (CFP) and *squares* (Aquamarine), and a series of pK_A values ranging from 5.0 to 6.2 was tested for the yellow acceptor (*continuous and dashed lines*). The experimental data for AKAR2.2 (*blue squares*) and Aqua-AKAR2.2 (*blues circles*) is reproduced from Fig. 3. All parameters used for the simulations are given in ESM Table S2

following analytical expression of the FRET ratio can be derived (see ESM):

$$R_{\mathrm{FRET}} = \frac{I_{\mathrm{bD}} + I_{\mathrm{dA}} + I_{\mathrm{sA}}}{I_{\mathrm{D}}} = f_{12} f_{\mathrm{DD}} \left[1 + f_{\mathrm{AD}} \frac{\frac{\mathrm{OD_A}}{\mathrm{OD_D}} + E_{\mathrm{FRET}}}{\frac{\Phi_{\mathrm{A}}}{\Phi_{\mathrm{D}}} (1 - E_{\mathrm{FRET}})} \right] \quad (2)$$

where f_{12}, f_{DD}, and f_{AD} are dimensionless spectral ratios which depend on both the instrumental settings (particularly the spectral bandwidths of detection) and the donor and acceptor emission spectral band shapes (see their detailed expression in ESM); E_{FRET} is the FRET efficiency; Φ_{D} and Φ_{A} are the fluorescence quantum yields of the donor and the acceptor in the absence of FRET; and $\mathrm{OD_A}/\mathrm{OD_D}$ is the ratio of their absorbances integrated over the excitation bandwidth. Equation (2) bears useful practical meanings that are discussed in the ESM. Notably, if the intrinsic photophysical properties of the donor and acceptor fluorophores remain unperturbed, R_{FRET} is a monotonous growing function of E_{FRET} and a linear function of $E_{\mathrm{FRET}}/(1-E_{\mathrm{FRET}})$ (Eq. S24).

In the case of pH changes that modify the intrinsic absorption and fluorescence properties of the cyan donor and the yellow acceptor, R_{FRET} will undergo more complex variations. Assuming that we can neglect the changes in fluorophore spectral band shapes, the only pH-dependent quantities in Eq. 2 are E_{FRET}, $\Phi_{\mathrm{A}}/\Phi_{\mathrm{D}}$, and $\mathrm{OD_A}/\mathrm{OD_D}$. These terms can be evaluated consistently with previous FLIM modeling:

$$E_{\mathrm{FRET}}(\mathrm{pH}) = \frac{k_{\mathrm{FRET}}}{k_{\mathrm{D}} + k_{\mathrm{FRET}}} = \frac{1}{\frac{1}{\tau_{\mathrm{D}}(\mathrm{pH}) k_{\mathrm{FRET}}(\mathrm{pH})} + 1} \quad (3a)$$

$$\frac{\Phi_{\mathrm{A}}}{\Phi_{\mathrm{D}}}(\mathrm{pH}) = \frac{\Phi_{\mathrm{A}}^{\mathrm{basic}}}{\Phi_{\mathrm{D}}^{\mathrm{basic}}} \times \frac{\tau_{\mathrm{D}}^{\mathrm{basic}}}{\tau_{\mathrm{D}}(\mathrm{pH})} \quad (3b)$$

$$\frac{\mathrm{OD_A}}{\mathrm{OD_D}}(\mathrm{pH}) = \alpha_{\mathrm{AD}} \frac{\varepsilon_{\mathrm{A}}^{\mathrm{basic}}}{\varepsilon_{\mathrm{D}}^{\mathrm{basic}}} \times \frac{1}{1 + 10^{(\mathrm{pK_A} - \mathrm{pH})}} \quad (3c)$$

where ${\Phi_{\mathrm{A}}}^{\mathrm{basic}}/{\Phi_{\mathrm{D}}}^{\mathrm{basic}}$ and ${\varepsilon_{\mathrm{A}}}^{\mathrm{basic}}/{\varepsilon_{\mathrm{D}}}^{\mathrm{basic}}$ are the ratios of acceptor to donor fluorescence quantum yields and molar absorption coefficients determined at basic pH levels, and α_{AD} is a constant spectral ratio evaluated from the normalized absorption bands of the cyan donor and the yellow anion acceptor. All these parameters can be estimated from solution studies of the purified fluorescent proteins (see ESM Table S2).

From Eqs. (1), (2), and (3), we can then compute the theoretical variations of the FRET ratio as a function of pH. The results obtained for the CFP/Citrine pair of AKAR2.2, assuming $\mathrm{pK_D}$=6.6 and n_{Hill}=1.7 for the CFP donor and a range of $\mathrm{pK_A}$ values for the Citrine acceptor, are shown in Fig. 7. Although the theoretical evolution of R_{FRET} with pH can be non-monotonous in some cases (see model curve for $\mathrm{pK_A}$=5.0), we find that the general trend is in all cases a pronounced decrease of the FRET ratio when going from neutral to acid pH levels, consistently with the above experimental observations on AKAR and other FRET systems. As expected, these pH changes are also associated with marked deviations from the normal linear relationship between R_{FRET} and $E_{\mathrm{FRET}}/(1-E_{\mathrm{FRET}})$ (see ESM Fig. S3).

Therefore, our model is able to qualitatively account for the observed FLIM and ratiometric responses of several FRET systems upon changes in pH. Yet, we find that Aqua-AKAR2.2 substantially deviates from the expected behavior at acid pH levels (Fig. 6). Considering the remarkable pH stability of the Aquamarine signal in the donor-only construct Aqua-AKAR2.2(Y66A) (Fig. 3), the behavior of Aqua-AKAR2.2 at acid pH levels must stem from the interaction of Aquamarine with the Citrine acceptor, i.e., from some FRET mechanism. In the modeling of the FRET ratio of AKAR2.2 (Fig. 7), the best agreement between theory and experiment is achieved for a very low pK of the Citrine acceptor ($\mathrm{pK_A}$=5.0, which corresponds to ≈40 % decrease in R_{FRET}), a low $\mathrm{pK_A}$ value that would be compatible also with the FLIM data on AKAR2.2 (Fig. 6). Taken together, these results would suggest a perturbation of the Citrine protonation equilibrium upon fusion into the AKAR biosensor, leading to a stabilization of its anionic form down to acid pH levels. However, this appears inconsistent with the high $\mathrm{pK_A}$ determined for Citrine in the Aqua-Citrine tandem (Fig. 2), and moreover does not satisfactorily account for the anomalous FLIM data of Aqua-AKAR2.2 (Fig. 6). Alternatively, an increased FRET interaction at acid pHs might also arise, either from pH-induced changes in the biosensor conformation or from the tendency of AKAR biosensors to concentrate into dense granules at acid pH levels (see "Materials and

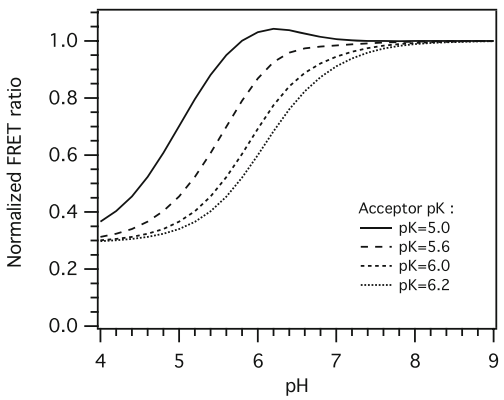

Fig. 7 Numerical simulations of the FRET ratio R_{FRET} at different pH levels for the AKAR2.2 biosensor. R_{FRET} at each pH was computed from Eq. (2) consistently with the simulations of Fig. 6 and was normalized to unity at basic pH. A series of different $\mathrm{pK_A}$ values ranging from 5.0 to 6.2 were tested for the acceptor (*continuous and dashed lines*). All parameters used for the simulations are given in ESM Table S2

methods"). This additional FRET contribution would decrease the fluorescence lifetime of the cyan donor below expected values (Fig. 6) and increase the FRET ratio above the predictions of our model (Fig. 7). We cannot exclude at the moment that several of the above hypotheses hold simultaneously, showing that still more investigations are required for a true quantitative description of the FRET signals of AKAR.

Conclusion

This work has revealed the major and complex impact of pH on the FLIM and ratiometric signals of a FRET biosensor carrying CFPs and YFPs in the living cell, which can be very significant in comparison to its functional response. Exchanging the CFP donor for a pH-insensitive Aquamarine does not eliminate these perturbations, but reveals instead the strong pH sensitivity of the yellow acceptor. As a general rule, most current genetically encoded FRET reporters cannot be used reliably in environments where the pH is expected to vary, especially in the acid range, like the secretory pathways.

There appears to be significant shifts in the transition pKs of fluorescent proteins when going from purified solution to the cytosolic environment. These shifts exceed the uncertainties in the absolute intracellular pH imposed by transmembrane ionophores [37]. Moreover, genetic fusion can in some cases substantially perturb the pH response of fluorescent proteins, as illustrated by the CFP donor of AKAR2.2. Mutations or truncations of the fluorescent protein, the nature of the anchoring sequence, and/or conformational changes within the biosensor might all contribute to these perturbations, which call for further investigations.

During this study, we have developed a consistent analytical model of FLIM and ratiometric experiments, which may be useful for future quantitative exploitation of intracellular FRET data in cytometry or imaging. We propose a physically grounded, explicit and simple relationship between the FRET ratio and the FRET efficiency (as measured by other techniques, like FLIM or pbFRET) that makes use of reasonably accessible spectral and photophysical information. The combination of ratiometric and spectral analysis with FLIM quantifications should help understanding more in depth the functioning of FRET biosensors in the living cell. The design of fully pH-insensitive FRET pairs would be also a major advance in the development of biosensors with extended domains of operation. Ultimately, routine methods for a specific in situ evaluation of FRET reporters regarding their pH stability could be settled and become part of the design process of all newly engineered biosensors.

Acknowledgments D.B.B. was the recipient of a doctoral grant from Region Ile-de-France (DIM Nanosciences IdF). We acknowledge supports from the Fondation pour la Recherche Médicale, the Centre National de la Recherche Scientifique through the program NEEDS and Paris-Sud University.

References

1. Newman RH, Fosbrink MD, Zhang J (2011) Genetically encodable fluorescent biosensors for tracking signaling dynamics in living cells. Chem Rev 111:3614–3666
2. Conway JRW, Carragher NO, Timpson P (2014) Developments in preclinical cancer imaging: innovating the discovery of therapeutics. Nat Rev Cancer 14:314–328
3. Shaner NC, Patterson GH, Davidson MW (2007) Advances in fluorescent protein technology. J Cell Sci 120:4247–4260
4. Kneen M, Farinas J, Li Y, Verkman AS (1998) Green fluorescent protein as a noninvasive intracellular pH indicator. Biophys J 74: 1591–1599
5. Llopis J, McCaffery JM, Miyawaki A, Farquhar MG, Tsien RY (1998) Measurement of cytosolic, mitochondrial, and Golgi pH in single living cells with green fluorescent proteins. Proc Natl Acad Sci 95:6803–6808
6. Wachter RM, Yarbrough D, Kallio K, Remington SJ (2000) Crystallographic and energetic analysis of binding of selected anions to the yellow variants of green fluorescent protein. J Mol Biol 301:157–171
7. Esposito A, Gralle M, Dani MAC, Lange D, Wouters FS (2008) pHlameleons: a family of FRET-based protein sensors for quantitative pH imaging. Biochemistry 47:13115–13126
8. Bencina M (2013) Illumination of the spatial order of intracellular pH by genetically encoded pH-sensitive sensors. Sensors 13: 16736–16758
9. Dupre-Crochet S, Erard M, Nusse O (2013) ROS production in phagocytes: why, when, and where? J Leukoc Biol 94:657–670
10. De Michele R, Carimi F, Frommer WB (2014) Mitochondrial biosensors. Int J Biochem Cell Biol 48:39–44
11. Salonikidis PS, Niebert M, Ullrich T, Bao G, Zeug A, Richter DW (2011) An ion-insensitive cAMP biosensor for long term quantitative ratiometric fluorescence resonance energy transfer (FRET) measurements under variable physiological conditions. J Biol Chem 286:23419–23431
12. Krause K-H, Milos M, Luan-Rilliet Y, Lew DP, Cox JA (1991) Thermodynamics of cation binding to rabbit skeletal muscle calsequestrin. J Biol Chem 266:9453–9459
13. Casey JR, Grinstein S, Orlowski J (2010) Sensors and regulators of intracellular pH. Nat Rev Mol Cell Biol 11:50–61
14. Lang F, Hoffmann EK (2012) Role of ion transport in control of apoptotic cell death. Compr Physiol 2:2037–2061
15. Lipton P (1999) Ischemic cell death in brain neurons. Physiol Rev 79:1431–1568
16. Markwardt ML, Kremers G-J, Kraft CA, Ray K, Cranfill PJC, Wilson KA, Day RN, Wachter RM, Davidson MW, Rizzo MA (2011) An improved cerulean fluorescent protein with enhanced brightness and reduced reversible photoswitching. PLoS One 6: e17896
17. Goedhart J, von Stetten D, Noirclerc-Savoye M, Lelimousin M, Joosen L, Hink MA, van Weeren L, Gadella TWJ, Royant A (2012) Structure-guided evolution of cyan fluorescent proteins towards a quantum yield of 93 %. Nat Commun 3:751
18. Erard M, Fredj A, Pasquier H, Betolngar D-B, Bousmah Y, Derrien V, Vincent P, Merola F (2013) Minimum set of mutations needed to optimize cyan fluorescent proteins for live cell imaging. Mol Biosyst 8:258–267

19. Mérola F, Fredj A, Betolngar D-B, Ziegler C, Erard M, Pasquier H (2014) Newly engineered cyan fluorescent proteins with enhanced performances for live cell FRET imaging. Biotechnol J 9:180–191
20. Grailhe R, Merola F, Ridard J, Couvignou S, Le Poupon C, Changeux JP, Laguitton-Pasquier H (2006) Monitoring protein interactions in the living cell through the fluorescence decays of the cyan fluorescent protein. ChemPhysChem 7:1442–1454
21. Thomas JA, Buchsbaum RN, Zimniak A, Racker E (1979) Intracellular pH measurements in Ehrlich ascites tumor cells utilizing spectroscopic probes generated in situ. Biochemistry 18:2210–2218
22. Poea-Guyon S, Ammar MR, Erard M, Amar M, Moreau AW, Fossier P, Gleize V, Vitale N, Morel N (2013) The V-ATPase membrane domain is a sensor of granular pH that controls the exocytotic machinery. J Cell Biol 203:283–298
23. Han J, Loudet A, Barhoumi R, Burghardt RC, Burgess K (2009) A ratiometric pH reporter for imaging protein-dye conjugates in living cells. J Am Chem Soc 131:1642–1643
24. Poea-Guyon S, Pasquier H, Mérola F, Morel N, Erard M (2013) The enhanced cyan fluorescent protein: a sensitive pH sensor for fluorescence lifetime imaging. Anal Bioanal Chem 405:3983–3987
25. Polito M, Vincent P, Guiot E (2014) Biosensor imaging in brain slice preparations. Methods Mol Biol 1071:175–194
26. Wachter RM, Remington SJ (1999) Sensitivity of the yellow variant of green fluorescent protein to halides and nitrate. Curr Biol 9: R628–R629
27. Griesbeck O, Baird GS, Campbell RE, Zacharias DA, Tsien RY (2001) Reducing the environmental sensitivity of yellow fluorescent protein. Mechanism and applications. J Biol Chem 276: 29188–29194
28. Nagai T, Ibata K, Park ES, Kubota M, Mikoshiba K, Miyawaki A (2002) A variant of yellow fluorescent protein with fast and efficient maturation for cell-biological applications. Nat Biotechnol 20:87–90
29. Fredj A, Pasquier H, Demachy I, Jonasson G, Levy B, Derrien V, Bousmah Y, Manoussaris G, Wien F, Ridard J, Erard M, Merola F (2012) The single T65S mutation generates brighter cyan fluorescent proteins with increased photostability and pH insensitivity. PLoS One 7:e49149
30. Nakabayashi T, Oshita S, Sumikawa R, Sun F, Kinjo M, Ohta N (2012) pH dependence of the fluorescence lifetime of enhanced yellow fluorescent protein in solution and cells. J Photochem Photobiol Chem 235:65–71
31. Bregestovski P (2009) Genetically encoded optical sensors for monitoring of intracellular chloride and chloride-selective channels activity. Front Mol Neurosci. doi:10.3389/neuro.02.015.2009
32. Dunn TA, Wang C-T, Colicos MA, Zaccolo M, DiPilato LM, Zhang J, Tsien RY, Feller MB (2006) Imaging of cAMP Levels and protein kinase a activity reveals that retinal waves drive oscillations in second-messenger cascades. J Neurosci 26:12807–12815
33. Depry C, Allen MD, Zhang J (2011) Visualization of PKA activity in plasma membrane microdomains. Mol Biosyst 7:52–58
34. Hoppe A, Christensen K, Swanson JA (2002) Fluorescence resonance energy transfer-based stoichiometry in living cells. Biophys J 83:3652–3664
35. Van Rheenen J, Langeslag M, Jalink K (2004) Correcting confocal acquisition to optimize imaging of fluorescence resonance energy transfer by sensitized emission. Biophys J 86:2517–2529
36. Zeug A, Woehler A, Neher E, Ponimaskin EG (2012) Quantitative intensity-based FRET approaches—a comparative snapshot. Biophys J 103:1821–1827
37. Boyarsky G, Hanssen C, Clyne LA (1996) Superiority of in vitro over in vivo calibrations of BCECF in vascular smooth muscle cells. FASEB J 10:1205–1212

Analytical and Bioanalytical Chemistry

Electronic Supplementary Material

pH sensitivity of FRET reporters based on cyan and yellow fluorescent proteins

Dahdjim-Benoît Betolngar, Marie Erard, Hélène Pasquier, Yasmina Bousmah, Awa Diop-Sy, Elvire Guiot, Pierre Vincent, Fabienne Mérola

Table S1. Experimental pKs and Hill coefficients obtained from FLIM measurements of cytosolic FRET tandems and AKAR biosensors (Figures 2 and 3). The parameters were obtained by directly fitting the variations with pH of the fluorescence lifetimes with cooperative transition models according to Equation S1.

Construct	Fluorophore	$pK_{1/2}$ ± Std Dev		n_{Hill}± Std Dev	
ECFP-EYFP(Y66A)	ECFP(1)	6.10	0.07	1.24	0.30
ECFP	ECFP(1)	6.27	0.22	0.71	0.35
AKAR2.2(Y66A)	CFP	6.58	0.02	1.67	0.17
Aqua-EYFP	EYFP(2)	6.72	0.09	1.12	0.24
Aqua-Citrine	Citrine(2)	6.23	0.10	1.25	0.41
Aqua-AKAR2.2	Citrine(2,3)	6.31	0.20	x	x

(1) The simultaneous fit of both data sets gives $pK_{1/2}$=6.2, which was used for FLIM modeling (Table S2).

(2) assuming that Aquamarine is insensitive to pH

(3) fit of the faint transition observed at mildly acid pHs.

Table S2. Experimentally derived parameters used for the modeling of FLIM and ratiometric data (Figures 5, 6 and 7)

Parameter	Modelled construct			
	ECFP-EYFP tandem	Aqua-EYFP/Cit tandem	AKAR2.2 biosensor	Aqua-AKAR2.2 biosensor
τ_{DA}^{basic} (1) (ns)	1.7	2.4	1.9	2.8
τ_{D}^{basic} (2) (ns)	2.4	3.9	2.4	3.9
τ_{D}^{acid} (2) (ns)	1.5	1.3	1.3	1.3
pK_D (3)	6.2	3.3	6.6	3.3
n_{Hill} (3)	1	1	1.7	1
f_{AD}			3.65 (4)	
α_{AD}			0.0264 (5)	
Φ_{A}^{basic}			0.76 (6)	
Φ_{D}^{basic} (7)			0.37 (7)	
ε_{A}^{basic} (M^{-1} cm^{-1})			80000 (6)	
ε_{D}^{basic} (M^{-1} cm^{-1})			30000 (8)	

(1) From the data of Figures 2 and 3.

(2) From donor only controls (Figures 2 and 3), estimates for Aquamarine at acid pH.

(3) From Table S1, estimates for Aquamarine.

(4) Computed from the emission spectra of the corresponding purified proteins, normalized to unit surface, and integrated over the transmission range of the yellow emission band pass filter.

(5) Computed from absorption spectra of the corresponding purified proteins, normalized to unit peak absorbance and integrated over the transmission range of the excitation band pass filter. The computation also assumes a flat illumination lamp spectrum. In the case of an excitation by an HBO lamp (strong mercury line at 436 nm), or by a SOLA lamp (showing large intensity variations over the transmission range of the filter) the value of α_{AD} becomes respectively 0.0269 and 0.0276, i.e. differs by less than 5% from a flat spectrum calculation.

(6) From [1].

(7) Determined at 20°C in 30 mM CAPS, 30mM MES and 30 mM Bis-trispropane, pH7.4 with Coumarin 510 in ethanol as reference, according to :

$$\Phi = \Phi_{ref} \frac{I_f}{I_f^{ref}} \frac{(1-10^{-OD_{ref}})}{(1-10^{-OD})} \left(\frac{n}{n_{ref}} \right)^2$$

where the emission intensity I_f was calculated from the spectrum area and OD is the absorbance at the excitation wavelength (420 nm). The fluorescence quantum yield of Coumarin 510 in ethanol was determined as $\Phi_{c510} = 0.74 \pm 0.01$ at 20°C using a cyclohexan solution of perylene as a standard ($\Phi_{perylene}$ in cyclohexane = 0.94, Berlman, I. B. (1965), Academic Press). As refractive index, we used $n_{ethanol} = 1{,}3614$, $n_{cyclohexane} = 1{,}4262$ and $n_{buffer} = 1{,}333$. (Reichardt, C. (1990), "Solvents and Solvent effects in Organic Chemistry", VCH, 2nd Ed.). Estimated SD = 0.02.

(8) From [2].

1. Absorption and fluorescence properties of purified EYFP and Citrine at different pHs and chloride concentrations.

We reinvestigated in depth the absorption properties of purified EYFP and Citrine in the presence of 0 to 600mM KCl, and at pHs comprised between pH 2.5 and pH 11. A typical series of spectra obtained for EYFP at different pHs in the presence of 83mM KCl, is shown in Figure S1a. Both EYFP and Citrine display, in addition to the absorption band of their aromatic amino acids at 280 nm, two absorption peaks at 392±2nm and 514±1nm, respectively ascribed to the neutral and anionic forms of their yellow chromophore. As previously reported [3, 4], the absorption intensity of both proteins at 514 nm decreases with decreasing pH, while their absorption at 392 nm increases. The observation of a neat isosbestic point at 438 nm indicates little interference with other spectroscopically active species. The fit of both neutral and anionic chromophore absorption band intensities gives identical $pK_{1/2}$s, with Hill coefficients close to 1.

For both proteins, the shape of the normalized absorption and emission spectral bands remains unchanged along the whole transition (data not shown). We also verified that KCl up to 600 mM concentration does not induce any detectable quenching of the fluorescence. A comparison of the absorption spectrum and the fluorescence excitation spectrum (with emission fixed at 530 nm) confirms that the neutral form is essentially non-fluorescent. Note also that the absorption spectrum of the neutral form does not extend above 450nm, and thus does not significantly overlap with the ECFP emission. Therefore the neutral form of yellow fluorescent proteins is a completely "dark" species in the FRET system, and neither contributes to the yellow fluorescence intensity nor acts as an energy transfer acceptor for cyan donors.

The fluorescence signal of purified EYFP and Citrine closely follows the loss in anion absorption (Figure S1). However, we found that their fluorescence lifetime, as

measured by TCSPC-FLIM decreases at acid pHs (Figure S2). This pH-induced quenching takes place at about one pH unit below the half-transition point for chromophore protonation. Accordingly, the quantum yield and fluorescence intensity of EYFP and Citrine would be decreased by 21% and 33% respectively at pH 5, as compared to their unquenched value at pH 7.4. This acid induced quenching has no incidence on donor lifetime modeling (which does not depend on the acceptor quantum yield), but may imply some correction to the effective FRET ratio R_{FRET} at very acid pHs (see Equations S17 and S23 below).

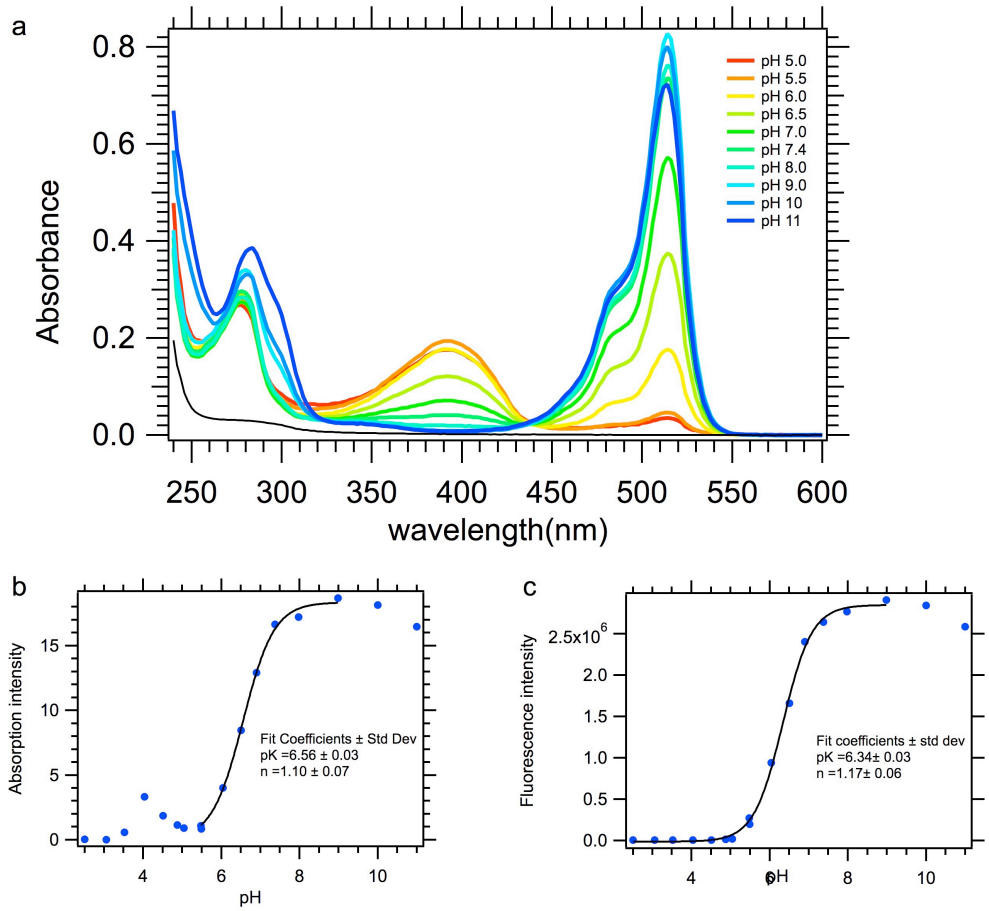

Figure S1. Absorption spectra of purified EYFP and study of its chromophore protonation equilibrium. (a) Absorption spectra of EYFP at different pHs in the presence of 83mM chloride concentration. (b) Evolution of the absorption intensity at 514 nm. (c) Evolution of the fluorescence intensity excited at 480 nm and integrated between 515 nm and 650nm. At pHs < 5, the absorption spectra include strong contributions from light scattering, which are maximum around pH 4 (Figure S1b). The anion absorption and fluorescence intensities also decrease slightly above pH 9 (Figures S1b and S1c), without any sign of turbidity (Figure S1a). Between pH 5 and pH 9, the amplitude of the absorption bands is well described by a cooperative Henderson-Hasselbalch transition model (continuous line) according to :

$$I_{Abs}(pH) = \frac{I_{Abs}^{basic} + I_{Abs}^{acid} \times 10^{n_{Hill}(pK_{1/2} - pH)}}{1 + 10^{n_{Hill}(pK_{1/2} - pH)}} \qquad \text{(S1)}$$

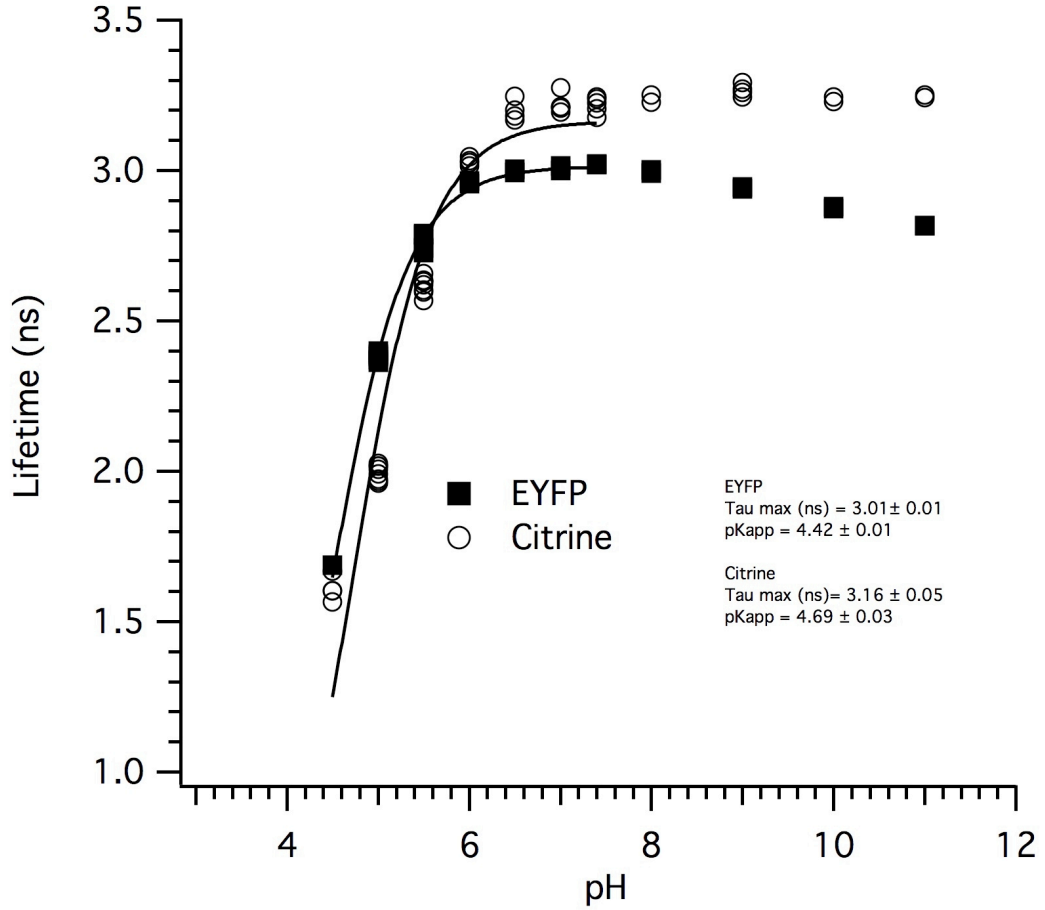

Figure S2. Average fluorescence lifetimes of purified EYFP and Citrine as a function of pH. The average lifetimes were determined by TCSPC-FLIM in the absence of chloride anions. Measurements at pHs below 4.5 were not possible due to the very low fluorescence intensity of the samples. The continuous lines represent the fitting of the corresponding data points to a simple transition model.

2. pH-dependent FRET model : development and discussion

The data presented in Figures 5 to 7 (Main Text) and S3 are based on a common model describing FRET between two pH-sensitive chromophores, under several approximations that can apply to CFPs and YFPs : the general frame of this model is to consider that acid pH effects are dominated on one hand by the loss in fluorescence quantum yield and lifetime of the CFP donor, and on the other hand by the loss in absorbance of the YFP acceptor.

The model relies first on the fundamentals of Förster resonant energy transfer (Section 2a). Modeling the CFP donor fluorescence lifetimes τ_D(pH) and τ_{DA}(pH) is based on a few minimal approximations (Section 2b). Consistently modeling the FRET ratio then requires further hypotheses and input information (Section 2c).

2a. General FRET principles

In the presence of a FRET interaction between a donor D and an acceptor A, the donor excited state lifetime is decreased due to the FRET deexcitation process :

$$\tau_D = \frac{1}{k_D} \qquad \text{in the absence of FRET}$$

$$\tau_{DA} = \frac{1}{k_D + k_{FRET}} \quad \text{with} \quad k_{FRET} = k_D \left(\frac{R_0}{R} \right)^6 \qquad \text{in the presence of FRET} \qquad \text{(S2)}$$

$$k_{FRET} = \frac{1}{\tau_{DA}} - \frac{1}{\tau_D}$$

where τ_D and τ_{DA} are the donor fluorescence lifetimes in the absence and presence of the acceptor, respectively, and k_{FRET} is the energy transfer rate constant.

According to Förster theory, k_{FRET} is given by :

$$k_{FRET} = \frac{1}{\tau_D}\frac{0.211^6 n^{-4}\kappa^2 \Phi_D J(\lambda)}{R^6} = \frac{0.211^6 n^{-4}\kappa^2}{R^6} \times \frac{\Phi_D}{\tau_D} \times J(\lambda)$$
$$k_{FRET} = \frac{0.211^6 n^{-4}\kappa^2}{R^6} \times k_R \times J(\lambda) \quad \text{(S3)}$$

where n is the refractive index, κ the orientation factor, R the distance separating the donor and the acceptor, Φ_D and τ_D the donor fluorescence quantum yield and lifetime respectively, whose ratio gives k_R, the donor radiative rate [5]. $J(\lambda)$ is the overlap integral given by :

$$J(\lambda) = \int f_D(\lambda)\ \varepsilon_A(\lambda)\lambda^4 d\lambda$$
$$= \varepsilon_A^{Max} \int f_D(\lambda)\ \alpha_N(\lambda)\ \lambda^4 d\lambda \quad \text{(S4)}$$
$$= \varepsilon_A^{Max} \times J_N$$

Where $f_D(\lambda)$ is the donor emission spectrum normalized to unit surface and $\alpha_N(\lambda)$ is the acceptor absorption spectrum normalized to unit peak absorbance.

The energy transfer rate k_{FRET} can thus be written as :

$$k_{FRET} = K \times \varepsilon_A^{Max} \quad \text{with} \quad K = \frac{0.211^6 n^{-4}\kappa^2}{R^6} k_R J_N \quad \text{(S5)}$$

k_{FRET} is thus proportional to the acceptor absorbance, but is independent of the donor fluorescence lifetime and quantum yield. We will assume that the donor radiative rate k_R remains constant under all experimental conditions, which appears to be approximately verified for CFPs [2, 6].

2b. Principles of τ_D(pH) and τ_{DA}(pH) modelling

For fluorescence lifetime modeling, the model neglects the small perturbations in donor absorption and emission spectral band shapes taking place at acid pHs [2], and takes advantage of the unchanged spectral band shape of acceptor absorption. If there is no change with pH in the relative donor-acceptor spatial configuration, the proportionality factor K of Equation S5 does not depend on pH and can be obtained by a

set of donor lifetime measurements in the absence and presence of the acceptor at basic pH :

$$K = \frac{k_{FRET}^{basic}}{\varepsilon_A^{basic}} = \frac{\left(\frac{1}{\tau_{DA}^{basic}} - \frac{1}{\tau_D^{basic}} \right)}{\varepsilon_A^{basic}} \quad \text{(S6)}$$

The pH dependence of acceptor absorbance is described by :

$$\varepsilon_A(pH) = \frac{\varepsilon_A^{basic}}{1+10^{(pK_A - pH)}} \quad \text{(S7)}$$

The pH dependence of the donor lifetime is described by :

$$\tau_D(pH) = \frac{\tau_D^{basic} + 10^{n_{Hill}*(pK_D - pH)}\ \tau_D^{acid}}{1+10^{n_{Hill}*(pK_D - pH)}} \quad \text{(S8)}$$

Main Text Equ (1a)

Equations S5, S6 and S7 lead to the following expression for the pH dependence of k_{FRET} :

$$k_{FRET}(pH) = \frac{\left(\frac{1}{\tau_{DA}^{basic}} - \frac{1}{\tau_D^{basic}} \right)}{1+10^{(pK_A - pH)}} \quad \text{(S9)}$$

Main Text Equ (1b)

According to Equation S2, the pH dependence of the donor fluorescence lifetime in the FRET system is thus given by :

$$\tau_{DA}(pH) = \frac{1}{\frac{1}{\tau_D(pH)} + k_{FRET}(pH)} \quad \text{(S10)}$$

Main Text Equ (1c)

The FRET efficiency E_{FRET} can be similarly obtained :

$$E_{FRET}(pH) = \frac{k_{FRET}}{k_D + k_{FRET}} = \frac{1}{\frac{1}{\tau_D(pH)\ \ k_{FRET}(pH)} + 1} \quad \text{(S11)}$$

Note that contrary to the energy transfer rate k_{FRET}, the FRET efficiency depends on both the acceptor absorbance and the donor fluorescence lifetime. If τ_D(pH) and k_{FRET}(pH)

both decrease when the pH decreases, E_{FRET} will also decrease, as a consequence of the simultaneous quenching of the donor and disappearance of the acceptor.

2c. Expression of the FRET ratio $R_{FRET}(pH)$

i. Components of the signal :

The FRET ratio R_{FRET} is determined by dividing the fluorescence intensities I_1 and I_2 measured in two separate spectral channels 1 and 2 more specific of the "donor" and the "acceptor" respectively, while exciting the FRET system near the maximum of donor absorption. In the case of CFPs and YFPs, provided an appropriate choice of the donor emission filter band pass (restricted to wavelengths below ≈ 500 nm), the intensity measured in the "donor" channel I_1 arises exclusively from the donor I_D. However, because of spectral overlaps, the intensity measured in the "acceptor" channel I_2 always comprises three significant contributions : the sensitized acceptor fluorescence I_{sA} due to FRET from the donor, the fluorescence from directly excited acceptors I_{dA}, and the bleed through of the donor I_{bD}, whose emission spectrum strongly overlaps the acceptor emission :

$$R_{FRET} = \frac{I_2}{I_1} = \frac{I_{bD} + I_{dA} + I_{sA}}{I_D} \qquad \text{(S12)}$$

The fluorescence intensity detected from a homogeneous fluorophore sample of quantum yield Φ_F can be expressed as :

$$I_F = \int_{\Delta\lambda_{exc}} I_{exc}(\lambda)\, T_{exc}(\lambda)\, OD_F(\lambda)\, d\lambda \quad \Phi_F \quad \int_{\Delta\lambda_{em}} f_F(\lambda)\, T_{em}(\lambda)\, Q_{\det}(\lambda)\, d\lambda \qquad \text{(S13)}$$

In this expression, the fluorophore absorbance spectrum $OD_F(\lambda)$ is weighted by the lamp intensity spectrum $I_{exc}(\lambda)$ and the transmission of the excitation filter $T_{exc}(\lambda)$ over the whole range of excitation wavelengths $\Delta\lambda_{exc}$, while the fluorophore emission spectrum normalized to unit surface $f_F(\lambda)$ is weighted by the transmission of the emission filter

$T_{em}(\lambda)$ and the detector sensitivity $Q_{det}(\lambda)$ over the range of detected emission wavelengths $\Delta\lambda_{em}$.

Assuming a flat lamp spectrum with intensity I_{exc} over the excitation range (the incidence of this approximation is evaluated in Table S2), a flat detector sensitivity Q_{det} over the emission range, and modern, square band pass filters with approximately constant transmissions T_{exc} and T_{em} over their operating wavelength range, allows the separation of instrumental and chromophore based contributions :

$$I_F = I_{exc}\ T_{exc}\ T_{em}\ Q_{\det} \int_{\Delta\lambda_{exc}} OD_F(\lambda)\ d\lambda \quad \Phi_F \int_{\Delta\lambda_{em}} f_F(\lambda)\ d\lambda \tag{S14}$$

The different contributions to the FRET ratio are then developed according to Equation S14, taking into account the FRET interaction, that transfers a fraction E_{FRET} of excitation quanta from the donor to the acceptor :

Donor Channel 1

$$I_D = I_{exc}\ T_{exc}\ T_{em1}\ Q_1 \int_{\Delta\lambda_{exc}} OD_D(\lambda)d\lambda \quad \Phi_D\left(1-E_{FRET}\right)\int_{\Delta\lambda 1} f_D(\lambda)d\lambda$$

Acceptor Channel 2

Donor bleed through

$$I_{bD} = I_{exc}\ T_{exc}\ T_{em2}\ Q_2 \int_{\Delta\lambda_{exc}} OD_D(\lambda)d\lambda \quad \Phi_D\left(1-E_{FRET}\right)\int_{\Delta\lambda 2} f_D(\lambda)d\lambda \tag{S15}$$

Direct acceptor

$$I_{dA} = I_{exc}\ T_{exc}\ T_{em2}\ Q_2 \int_{\Delta\lambda_{exc}} OD_A(\lambda)d\lambda \quad \Phi_A\int_{\Delta\lambda 2} f_A(\lambda)d\lambda$$

Sensitized acceptor

$$I_{sA} = I_{exc}\ T_{exc}\ T_{em2}\ Q_2 \int_{\Delta\lambda_{exc}} OD_D(\lambda)d\lambda \quad E_{FRET}\ \Phi_A\int_{\Delta\lambda 2} f_A(\lambda)d\lambda$$

$\Delta\lambda_{exc}$ being the range of excitation wavelengths and $\Delta\lambda 1$ and $\Delta\lambda 2$ being the range of detected emission wavelengths in channel 1 and channel 2 respectively.

ii. Expression of the FRET ratio R_{FRET}

From equations S12 and S15, the following expression is obtained for the FRET ratio :

$$R_{FRET} = \frac{T_{em2}\ Q_2}{T_{em1}\ Q_1} \frac{\int_{\Delta\lambda 2} f_D(\lambda) d\lambda}{\int_{\Delta\lambda 1} f_D(\lambda) d\lambda} \left(1 + \frac{\Phi_A}{\Phi_D} \frac{\int_{\Delta\lambda 2} f_A(\lambda) d\lambda}{\int_{\Delta\lambda 2} f_D(\lambda) d\lambda} \frac{\frac{\int_{\Delta\lambda_{exc}} OD_A(\lambda) d\lambda}{\int_{\Delta\lambda_{exc}} OD_D(\lambda) d\lambda} + E_{FRET}}{(1 - E_{FRET})} \right) \quad \text{(S16)}$$

which is re-written as Equation 2 (main text):

$$R_{FRET} = \mathrm{f_{12}} \mathrm{f_{DD}} \left[1 + \mathrm{f_{AD}} \frac{\Phi_A}{\Phi_D} \frac{\frac{OD_A}{OD_D} + E_{FRET}}{(1 - E_{FRET})} \right] \quad \text{(S17)}$$

(Main text Equ 2)

where the different spectral ratios f_{XY} are defined as follows :

- the spectral sensitivity ratio f_{12} corresponds to the relative detection efficiency in channel 1 and channel 2 :

$$\mathrm{f_{12}} = \frac{T_{em2}\ Q_2}{T_{em1}\ Q_1} \quad \text{(S18)}$$

- the donor spectral ratio f_{DD} measures the relative amount of donor photons collected within the detection spectral ranges of channel 1 and channel 2 :

$$\mathrm{f_{DD}} = \frac{\int_{\Delta\lambda 2} f_D(\lambda) d\lambda}{\int_{\Delta\lambda 1} f_D(\lambda) d\lambda} \quad \text{(S19)}$$

- the acceptor to donor spectral ratio f_{AD} is the relative fraction of acceptor and donor fluorescence photons collected within the spectral range of channel 2 :

$$f_{AD} = \frac{\int_{\Delta\lambda 2} f_A(\lambda) d\lambda}{\int_{\Delta\lambda 2} f_D(\lambda) d\lambda} \quad \text{(S20)}$$

- in the case of a fixed 1:1 stoechiometry, the absorption ratio OD_A/OD_D can be expressed as :

$$\frac{OD_A}{OD_D} = \frac{\varepsilon_A^{Max}}{\varepsilon_D^{Max}} \frac{\int_{\Delta\lambda_{exc}} \alpha_A^N(\lambda) d\lambda}{\int_{\Delta\lambda_{exc}} \alpha_D^N(\lambda) d\lambda} = \alpha_{AD} \frac{\varepsilon_A^{Max}}{\varepsilon_D^{Max}} \quad \text{(S21)}$$

where $\varepsilon^{Max}{}_A$ and $\varepsilon^{Max}{}_D$ are the acceptor and donor peak molar absorption coefficients respectively.

- the absorption spectral ratio α_{AD} is computed from the donor and acceptor absorption spectra normalized to unit peak absorbance integrated over the excitation spectral range $\Delta\lambda_{exc}$:

$$\alpha_{AD} = \frac{\int_{\Delta\lambda_{exc}} \alpha_A^N(\lambda) d\lambda}{\int_{\Delta\lambda_{exc}} \alpha_D^N(\lambda) d\lambda} \quad \text{(S21b)}$$

All spectral ratios f_{12}, f_{DD}, f_{AD}, and α_{AD} are constant parameters if the fluorophore spectral band shapes remain unchanged. When the relative variations of the FRET ratio $\Delta R/R$ are monitored, the terms outside the square bracket of Equation 2 (S17) cancel out, and the only spectral ratios that need to be evaluated are f_{AD} and α_{AD}. These parameters were approximated from experimental spectra obtained on the purified proteins (Table S2).

Then, the theoretical expression of the FRET ratio involves only three pH-dependent terms : the FRET efficiency E_{FRET}, the ratio of acceptor to donor quantum yields Φ_A/Φ_D, and the ratio of acceptor to donor absorbances OD_A/OD_D. All three terms can be described consistently with FLIM modelling. First, E_{FRET} is given by Equation S12 above.

Then, the absorbance ratio OD_A/OD_D is obtained through Equation S7, neglecting the small changes in donor absorbance ($\varepsilon_D^{Max} \approx cst$) :

$$\frac{OD_A}{OD_D} = \alpha_{AD} \frac{\varepsilon_A^{Max}(pH)}{\varepsilon_D^{Max}}$$

$$\frac{OD_A}{OD_D} = \alpha_{AD} \frac{\varepsilon_A^{basic}}{\varepsilon_D^{basic}} \times \frac{1}{1+10^{(pK_A-pH)}} \qquad \text{(S22)}$$

Finally, the quantum yield ratio Φ_A/Φ_D is obtained through Equation S8, neglecting the dynamic quenching of EYFP/Citrine fluorescence at acid pHs ($\Phi_A \approx cst$), and assuming proportionality between the donor fluorescence quantum yield and lifetime :

$$\frac{\Phi_A}{\Phi_D} = \frac{\Phi_A}{\Phi_D(pH)} = \frac{\Phi_A^{basic}}{\Phi_D^{basic}} \times \frac{\tau_D^{basic}}{\tau_D(pH)}$$

$$\frac{\Phi_A}{\Phi_D} = \frac{\Phi_A^{basic}}{\Phi_D^{basic}} \times \frac{1+10^{n_{Hill}*(pK_D-pH)}}{1+\tau_D^{acid}/\tau_D^{basic} \times 10^{n_{Hill}*(pK_D-pH)}} \qquad \text{(S23)}$$

2e. Discussion of the expression of the FRET ratio

1) Equation 2(S17) shows that, in the absence of photophysical perturbations of the fluorophores other than FRET changes, the FRET ratio is, as expected, a monotonous growing function of E_{FRET}. Moreover, the FRET ratio is a linear function of $E_{FRET}/(1-E_{FRET})$:

$$X = \frac{E_{FRET}}{1-E_{FRET}} \qquad E_{FRET} = \frac{X}{X+1}$$
$$R_{FRET} = \mathrm{f_{12}f_{DD}}\left[1+\mathrm{f_{AD}}\frac{\Phi_A}{\Phi_D}\left(\frac{E_{FRET}}{1-E_{FRET}}\left(\frac{OD_A}{OD_D}+1\right)+\frac{OD_A}{OD_D}\right)\right] \quad \text{(S24)}$$

2) An approximate prediction of the dependence of R_{FRET} on pH can also be inferred from Equation 2(S17). In the absence of direct acceptor excitation ($OD_A/OD_D=0$), the expression of R_{FRET} reduces to :

$$R_{FRET} \propto 1+\mathrm{f_{AD}}\frac{\Phi_A}{\Phi_D}\frac{E_{FRET}}{\left(1-E_{FRET}\right)}$$
$$\frac{E_{FRET}}{1-E_{FRET}} = \tau_D(pH) * k_{FRET}(pH)$$
$$\frac{\Phi_A}{\Phi_D} = \frac{\Phi_A^{basic}}{\Phi_D^{basic}}\frac{\tau_D^{basic}}{\tau_D(pH)} \quad \text{(S25)}$$

$$R_{FRET} \propto 1+\mathrm{f_{AD}}\frac{\Phi_A^{basic}\tau_D^{basic}}{\Phi_D^{basic}}k_{FRET}(pH)$$

In the approximation of no direct acceptor excitation, R_{FRET} thus becomes a simple linear function of k_{FRET}, whose pH dependence is in turn given by Equation S9. It can thus be expected that R_{FRET}, similarly to k_{FRET}, will decrease monotonously when the pH is decreased, and a negative variation ΔR/R is expected after a jump from neutral to acid pH. In other words, the behavior of R_{FRET} is strongly dominated, *via* $k_{FRET}(pH)$, by the loss in acceptor absorbance, and is less influenced by the pH-induced donor quenching, following the above cancellation of the $\tau_D(pH)$ term. Deviations from this simple behavior will arise from the presence of directly excited acceptor fluorescence I_{dA} in detection channel 2, giving rise to the (possibly) non monotonous product $(OD_A\Phi_A)/(\Phi_D OD_D)$ in the expression of R_{FRET}.

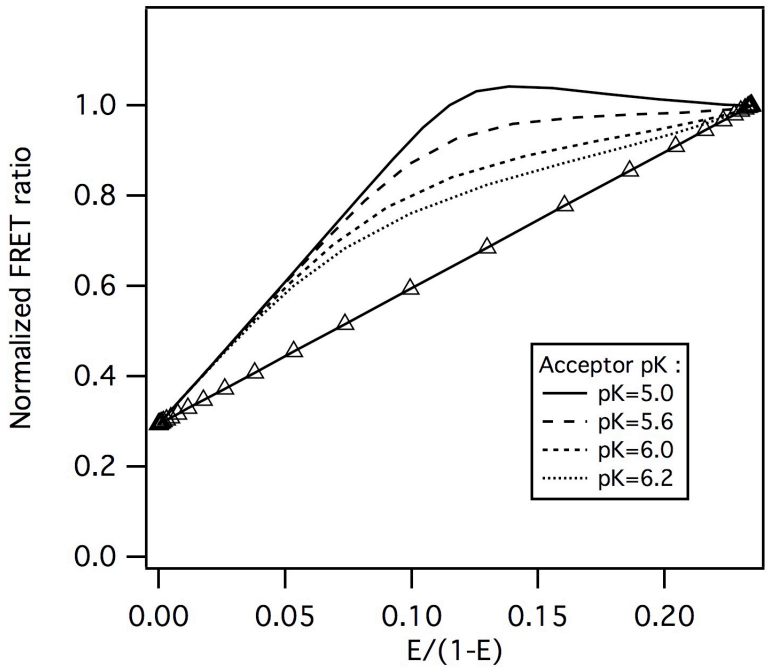

Figure S3. Non-linear relationship between R_{FRET} and $E_{FRET}/(1-E_{FRET})$ in the pH dependent models of Figure 7. The triangles correspond to the evolution of the FRET ratio assuming a pH dependent change of the FRET efficiency over the same interval, with the parameters Φ_A/Φ_D and OD_A/OD_D blocked at their values at basic pH.

References

1. Griesbeck O, Baird GS, Campbell RE, Zacharias D a, Tsien RY (2001) Reducing the environmental sensitivity of yellow fluorescent protein. Mechanism and applications. J Biol Chem 276:29188–29194.

2. Fredj A, Pasquier H, Demachy I, Jonasson G, Levy B, Derrien V, Bousmah Y, Manoussaris G, Wien F, Ridard J, Erard M, Merola F (2012) The single T65S mutation generates brighter cyan fluorescent proteins with increased photostability and pH insensitivity. PLoS One 7:e49149.

3. Wachter RM, Yarbrough D, Kallio K, Remington SJ (2000) Crystallographic and energetic analysis of binding of selected anions to the yellow variants of green fluorescent protein. J Mol Biol 301:157–71.

4. Sinnecker D, Voigt P, Hellwig N, Schaefer M (2005) Reversible Photobleaching of Enhanced Green Fluorescent Proteins. Biochemistry 44:7085–7094.

5. Valeur B (2001) Molecular Fluorescence Principles and Applications. Wiley-VCH, Weinheim

6. Villoing A, Ridhoir M, Cinquin B, Erard M, Alvarez L, Vallverdu G, Pernot P, Grailhe R, Mérola F, Pasquier H (2008) Complex fluorescence of the cyan fluorescent protein: comparisons with the H148D variant and consequences for quantitative cell imaging. Biochemistry 47:12483–12492